Research Article Vol. 3, No. 2 / 15 February 2020 / OSA Continuum 236

Transport of intensity equation based photon-counting phase imaging

ALOK K. GUPTA,[1] NAVEEN K. NISHCHAL,[1,*] AND PARTHA P. BANERJEE[2]

[1]Department of Physics, Indian Institute of Technology Patna, Bihta, Patna-801 106, India
[2]Department of Electro-Optics and Photonics, University of Dayton, 300 College Park, Dayton, Ohio 45469, USA
[*]nkn@iitp.ac.in

Abstract: In low light conditions, such as in astronomy and non-invasive bio-imaging applications, the imaging performance is mostly degraded due to noise. In this paper, we demonstrate a transport of intensity equation based technique that uses photon-counting phase imaging. To achieve the phase imaging in a photon starved condition, a method proposed by Paganin *et al.* [J. Micros. **214**, 51 (2004)] has been used. The method uses the fact that the magnitude of the wavefront curvature determines the quality of the recovered phase image for a given noise level and defocus distance. The effectiveness of the proposed method has been illustrated through simulations and experimental results using inexpensive partially coherent illumination. The study can find applications in non-invasive phase imaging.

1. Introduction

The methods of phase imaging have evolved many-fold in the last few decades. Phase objects have surface unevenness or difference in its refractive index with respect to its surroundings. There are several phase imaging techniques in the literature which include phase contrast [1], interferometric [2–6], iterative [7–10] and non-interferometric non-iterative techniques [11–19]. The phase imaging has been applied to many fields of scientific research including biomedical imaging [2], information security [3,6], astronomy [20], metrological applications [21]. Though interference-based techniques and iterative phase retrieval methods are well established for phase imaging but these methods typically rely on perfect coherence of light source, therefore, the phase aberration and coherent noise problem usually prevent the accurate and high quality phase images. However, incoherent digital holography has been reported to avoid such problems [22]. The transport of intensity equation (TIE) is a non-iterative and non-interferometric phase retrieval method, which is based on the intensity derivative of the object along the optic axis [11–13]. If we know the longitudinal intensity derivative in the near field region, the phase distribution can easily be computed numerically.

Imaging in low light has been a very challenging task due to receiving of low number of photons at image sensor [23–29]. The functioning of the electronic cameras and how the properties can be exploited to optimize image quality under low-light conditions has been studied [23]. In situations where the light source is weak the detection signal-to-noise ratio (SNR) is limited by the quantized nature of light. Imaging systems' performance at low light intensity is degraded, which becomes increasingly strong as the power of the light source decreases [29]. Therefore, shot noise contribution is proportionally higher in SNR calculations. Shot noise, which may often be modelled as Poisson noise, is the form of uncertainty associated with the measurement of light.

Usually in the image recording process, it is assumed that the illumination intensity of the light field does not influence the object. However, if the object is a biological organism or any photo-material, the illumination of the light field should be restricted as per the sample

#383527 https://doi.org/10.1364/OSAC.383527
Journal © 2020 Received 18 Nov 2019; revised 8 Jan 2020; accepted 9 Jan 2020; published 23 Jan 2020

OSA CONTINUUM

requirement. In such cases, methods for low light phase imaging need to be investigated. Similarly, in astronomy, where light from solar bodies is too weak, imaging of terrestrial bodies pose significant problem [20]. For retrieving phase information in such cases, the conventional phase retrieval methods such as computational ghost imaging (CGI), digital holography (DH), and iterative phase retrieval algorithms have been investigated. The method based on ghost imaging is also relatively slow because of large number of images are recorded [19]. Similarly, the digital holography based photon-counting imaging has some well-known problems like need of perfect coherence illumination and phase unwrapping issue [24]. The iterative phase retrieval methods are highly computational and time-consuming, and mainly depend on high performance computers [29].

The TIE is a kind of reference-less holography technique and has been reported perform well even with the use of partially coherent illumination [30–32]. TIE is experimentally easy and computationally efficient as compared to the conventional phase retrieval techniques. It has been reported that the separation between defocusing planes in the TIE, also known as defocused distance, should be chosen based on the noise level in the recording of image data,the noisier the data the greater the separation between the measurement planes in order to recover phase. Too small defocus distance implies that the reconstructed phase will be dominated by noise induced artifacts [33]. The small defocusing separation, as used in the conventional TIE, would not yield the significant phase information since it would be dominated by noise induced artefacts. Large defocusing distance in such conditions makes the intensity derivative signal to rise above the noise in the data. The phase sensitivity in noisy conditions can be maintained by using large defocusing based TIE.

In this paper, we utilize the property of large defocusing with noise in achieving the phase imaging in low light level condition through TIE. To create the low illumination level, photon-counting imaging has been employed with partially coherent light source such as a light emitting diode (LED). LED has been used because TIE is less sensitive to coherence of the illumination source [31,32]. Conventional TIE does not yield satisfactory results in low light illumination condition. Large defocusing based TIE has shown effectiveness in noisy conditions for maintaining phase sensitivity [33], which has been utilized here for photon-counting imaging.

2. Background theory

2.1. Phase imaging by the transport of intensity equation

The well-known TIE equation is given by [11–13],

$$\nabla_{\perp}[I_z(x,y)\cdot\nabla_{\perp}\phi_z(x,y)] = -\frac{2\pi}{\lambda}\frac{\partial I}{\partial z} \tag{1}$$

where λ is the wavelength of light source and $I_z(x,y)$ and $\phi_z(x,y)$ denote the intensity and phase distributions at a particular plane on the optical axis z, respectively. $\nabla_{\perp}$ denotes the gradient operator in transverse plane. The phase can be determined from differentiation of intensities at several planes in the near field region. The equation can be simplified as two-dimensional (2D) Poisson equation for solving the phase term [11]. For relating directly to phase distributions, Eq. (1) can be expanded as

$$\begin{aligned} -\tfrac{2\pi}{\lambda}\tfrac{\partial I}{\partial z} &= \nabla_{\perp}I_z(x,y)\cdot\nabla_{\perp}\phi_z(x,y,0) + I_z(x,y)\nabla_{\perp}^2\phi_z(x,y,0) \\ &\approx I_0\nabla_{\perp}^2\phi_z(x,y,0) \end{aligned} \tag{2}$$

where it is assumed that the intensity is nearly constant (and equal to I_0) such that the first term on the right hand side is small compared to the second term. Implications of this assumption are discussed in detail in Basunia *et al*. [16]. The intensity is assumed to be constant around the

OSA CONTINUUM

in-focus plane, consistent with a very weakly absorbing or non-absorbing thin sample. Rewriting the phase distribution at this plane as $\phi_0(x,y)$, Eq. (2) can be simplified as

$$\nabla_{\perp}^2 \phi_0(x,y) = -\frac{2\pi}{\lambda I_0}\frac{\partial I(x,y)}{\partial z} \tag{3}$$

which is the 2D Poisson equation, and can be easily solved by applying 2D fast Fourier transform (FFT) algorithm. Taking the Fourier transform of both sides,

$$-4\pi^2(k_x^2+k_y^2)\Phi_0(k_x,k_y) = -\frac{2\pi}{\lambda I_0}\Im\left[\frac{\partial I(x,y)}{\partial z}\right] \tag{4}$$

where Φ_0 denotes the Fourier transform of ϕ_0, k_x and k_y denote the spatial frequencies corresponding to the x and y axes, respectively. The Fourier transform and inverse Fourier transform operations are denoted by $\Im$ and $\Im^{-1}$, respectively. For solving the equation, the expression is inverse Fourier transformed [13]:

$$\phi_0(x,y) = \frac{2\pi}{\lambda I_0}\Im^{-1}\left[\frac{1}{4\pi^2(k_x^2+k_y^2)}\Im\left[\frac{\partial I(x,y)}{\partial z}\right]\right] \tag{5}$$

The intensity derivative dI/dz in Eq. (3) can be approximated by the finite difference method using the two defocused intensities at positions dz and $–dz$,

$$\frac{\partial I}{\partial z} \approx \frac{I_{dz}(x,y) - I_{-dz}(x,y)}{2dz} \tag{6}$$

Using the above equations, the phase distributions can be obtained directly with two defocused intensity distributions. The defocused image stacks are captured by translating the CCD camera along the optic axis.

2.2. Photon counting imaging

In conventional phase imaging techniques, light detection is performed by indirectly measuring high energy photons. The random nature of photon emission and detection are often the dominant source of noise in imaging [34]. When the number of the photons is small, the photon-counting detection is assumed to be Poisson distribution. The probability of counting n photons in a time interval can be shown to be Poisson distributed. The probability distributions can be defined by the following expression P as [35,36],

$$P(n;r,t) = \frac{[a(r)t]^n \exp[-a(r)t]}{n!}, \quad n = 1,\ 2,\ 3,\ \ldots \tag{7}$$

where, n is the total number of photons produced by detector centred on a position vector $\boldsymbol{r}$ during a time interval t and $a(r)$ is the rate parameter. $n_p = a(r)t$ represents mean of photon counts. The recorded irradiance on a pixel is related to the mean number of photons that arrive at that pixel. Hence, the photon-limited images can be simulated from recorded intensity images. The mean number of photons at a pixel at position r_i will be given by [36],

$$n_p(r_i) = \frac{N_p I_p(r_i)}{\sum_{j=1}^{N_T} I_p(r_j)} \tag{8}$$

where I_p is irradiance, N_T is total number of pixels, and N_p is the expected number of photons in the image. N_p has been changed to generate the photon counting images at different number of photons.

OSA CONTINUUM

In the actual experiment, the original objects have been illuminated by an LED light source and the image intensity distributions have been recorded by a CCD camera. The captured intensity distribution has been used for simulating the different photon counting levels. This is achieved through altering the value of N_p as expressed in Eq. (8) [35–38]. The sparse images are obtained after applying PC technique to all intensity images (focused, over-focused, and under-focused).

2.3. Effect of low light illumination in defocusing distance in TIE

It has been shown that the TIE with large defocusing can retrieve the phase information in noisy conditions [33]. Therefore, in this work we explore the PC imaging based on TIE with large defocusing. As we discussed earlier, low light illumination can be modelled as a Poisson distribution, usually known as photon noise or shot noise. The recovered phase image ϕ_0 is obtained solely by the intensity distribution I_0 and intensity derivative along the optic axis in the sensor plane dI/dz. Though numerically, the two quantities can be measured to a precision, the measurement is usually influenced by the level of noise in the experiment. The quantity dI/dz can be related to the noise in the TIE system.

Let us denote the defocused intensities images at two planes separated by I_{dz} and $I_{-\mathrm{dz}}$, and the focussed intensity as I_0. In actual experiment, the measurements in each of the measurement planes will be affected by system noise. Therefore, the noise term can be separated from the ideal noise free intensity distribution. Assuming the noise distribution to be statistically identical and independent of intensity distribution, the intensity distributions can be expressed as the sum of ideal noise-free intensity distribution I^{ideal} and a noise term σ [33],

$$\begin{aligned} I_{dz}(x,y) &= I_{dz}^{ideal}(x,y) + \sigma_{dz}(x,y) \\ I_{-dz}(x,y) &= I_{-dz}^{ideal}(x,y) + \sigma_{-dz}(x,y) \end{aligned} \tag{9}$$

Subtracting the intensity distributions, $I_{dz}(x,y)$ and $I_{-dz}(x,y)$, the Eq. (9) can be expressed as,

$$I_{dz}(x,y) - I_{-dz}(x,y) = [I_{dz}^{ideal}(x,y) - I_{-dz}^{ideal}(x,y)] + [\sigma_{dz}(x,y) - \sigma_{-dz}(x,y)] \tag{10}$$

Performing the cubic-order Maclaurin series expansion of I_{dz}^{ideal} about the zero defocus, subtracting the resulting pair of linear equations, and dividing by $2dz$,

$$\frac{I_{dz}(x,y) - I_{-dz}(x,y)}{2dz} = \frac{\partial I^{ideal}(x,y,0)}{dz} + \frac{dz^2}{3!}\frac{\partial^3 I^{ideal}(x,y,0)}{dz^3} + \frac{\sigma(x,y)}{\sqrt{2}dz} \tag{11}$$

The noise terms (σ_{dz} and σ_{-dz}) have been assumed to be statistically identical and therefore they have been combined in quadrature. The approximations can be sufficiently good for the purpose of investigating the effect of noise on the phase recovery. From Eqs. (2) and (11), and neglecting the third derivative, the following conditions must be satisfied.

$$\frac{2\pi}{\lambda I_0}\frac{\sigma}{\sqrt{2}dz} \langle\langle \left\langle \nabla_\perp^2 \phi_z(x,y) \right\rangle_{RMS} \tag{12}$$

$$\frac{k}{6I_0}\left\langle \frac{\partial^3 I_{ideal}(x,y,0)}{\partial z^3} \right\rangle_{RMS} dz^2 \langle\langle \left\langle \nabla_\perp^2 \phi_z(x,y) \right\rangle_{RMS} \tag{13}$$

This inequality is concerned with the noisy data and shows that the noisier the data the greater should be the separation between the defocusing planes. Too small defocus distance implies that the reconstructed phase will be dominated by noise induced artefacts. From Eq. (12), it could be thought that phase sensitivity can be arbitrarily increased by simply increasing the defocus distance, but it is true only up-to an extent that Eq. (13) is also satisfied. It can be concluded

OSA CONTINUUM

from Eqs. (12) and (13), that we have a trade-off between acceptable noise and defocus distance. For decreasing photon counts, the defocus distance has to be increased. In this study, the defocus distance from the image plane without photon counting is 0.1 mm. This defocus distance changes to 1.5 *mm* and 2.0 *mm*, respectively when photon counts (N_p) are 10^5, and 10^4, respectively. As for the TIE in Eq. (3) and the finite difference approximation as in Eq. (11), both the equations are good approximations for Fourier components in the phase that do not change significantly over the scale of the critical length. Waller *et al*. [11] demonstrated a method based on a better approximation of the first axial derivative of the intensity required in the TIE by estimating higher order derivatives for improving the accuracy of phase retrieval. This was achieved through using intensity measurements at multiple planes around the focus (or image plane). A method to obtain more accurate solutions for the phase by recursively using TIE and the associated transport of phase equation which results from the *eikonal* equations in the presence of diffraction has been discussed by Basunia *et al*. [16].

3. Results and discussion

We explain here experimental and numerical methodology for demonstration of the TIE with large defocusing based photon counting imaging. First, we record the intensity information required for the TIE without neutral density filter (NDF) to ensure sufficiently high photon numbers to correspond to an essentially noise free image, which will later be compared to photon starved images obtained using a strongly attenuating neutral density filter. The intensities are then processed with Poisson distribution based photon counting method, where we numerically reduced the number of photons up to 10^5 and 10^4, respectively. These processed intensity stacks (or 'sparsed images') are utilized for TIE. The conventional TIE is not able to retrieve the phase information in such photon-limited conditions, but significant improvement can be achieved by the large defocusing based TIE. This has been verified experimentally using NDF for decreasing the illumination level in the intensity recording. Detailed explanations are given in the following subsections.

3.1. Numerical simulations

Numerical simulation has been carried out to illustrate the ability of TIE phase imaging in photon-limited condition. The pixel size of the images used in the simulation is 1024×1024 pixels. The required image stacks have been sparsed using photon counting method. The obtained focussed, under-focussed and over-focussed images have been independently made sparser to mimic the low light illumination situation. The phase recovery has been done using FFT-based TIE solver. The effect of singularity in Eq. (5) can be mitigated using the technique outlined in, for instance, Basunia *et al*. [13]. In the simulations examples shown in Figs. 1 and 2, Figs. 1(a), 2(a) show the original images of a micro-lens and a micro-lens array, respectively, without photon limiting. For the photon-limited case, the number of photons has been taken as 10^5 in Figs. 1(b), 2(b), and 10^4 in 1(c), 2(c), respectively. We have to take sufficiently larger defocus distance while solving TIE, since FFT-based TIE solver has a property to retrieve phase in noisy conditions by sufficiently increasing the defocusing distance.

3.2. Experimental results and analysis

The schematic diagram shown in Fig. 3 depicts the experimental setup. A low cost red LED source (central wavelength 629.4 nm, FWHM 13.1 nm) has been used as the illumination source. A variable NDF has been placed after the condenser lens (135 mm focal length) for varying the intensity of illumination source. The illumination beam is passed through the phase object. A combination of 10X microscope objective and 75 mm lens has been used to magnify the micro phase object at the image plane. Then the magnified image has been relayed through a 4*f* imaging system to a CCD camera (make: Imaging Source, number of pixels: 2592×1944, pixel size 2.2

OSA CONTINUUM

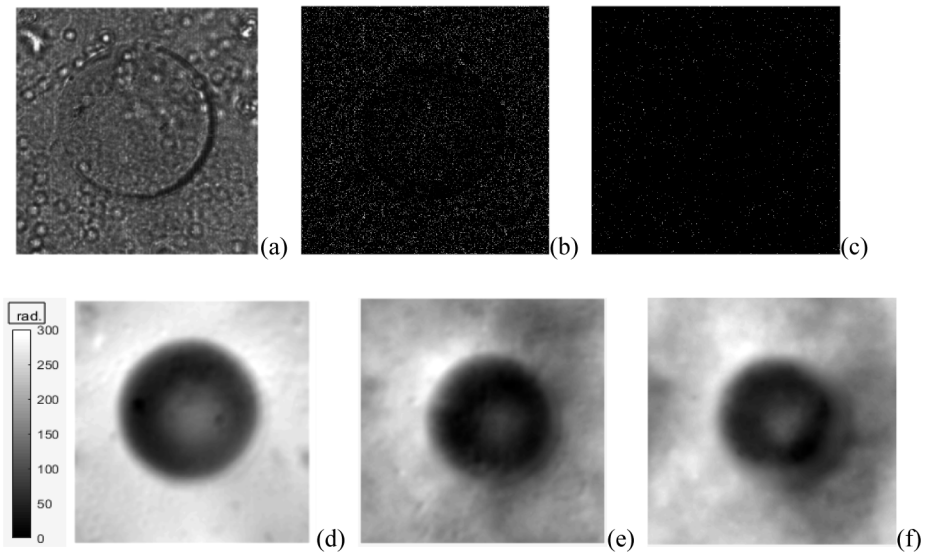

Fig. 1. Focussed intensity image of micro-lens (a) without photon-limiting, (b) photon-limited with $N_p = 10^5$, (c) photon-limited with $N_p = 10^4$, (d), (e), and (f) show their retrieved phase, respectively.

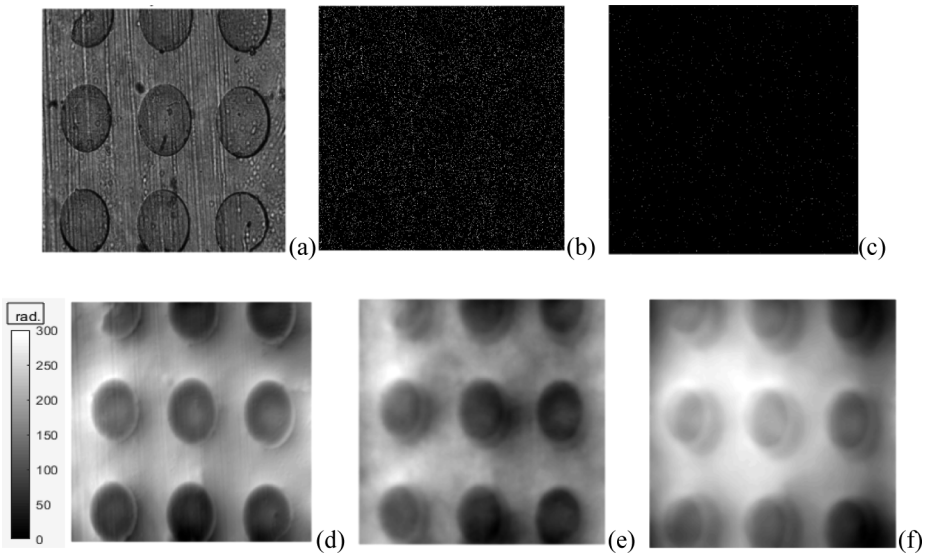

Fig. 2. Focussed intensity image of micro-lens array (a) without photon-limiting, (b) photon-limited with $N_p = 10^5$, (c) photon-limited with $N_p = 10^4$,(d), (e), and (f) show their retrieved phase, respectively.

$\times$ 2.2 µm). The camera is placed on a motorized translation stage controlled through a personal computer.

A single micro-lens, a micro-lens array (both used also in simulations above), and an onion's peel have been used as pure phase objects. The NDF has been varied such that the corresponding SNR in intensity has been reduced to average value of 7.2 and 6.7, respectively. At such low SNR levels, the TIE in large defocusing condition can yield significant phase information, as

OSA CONTINUUM

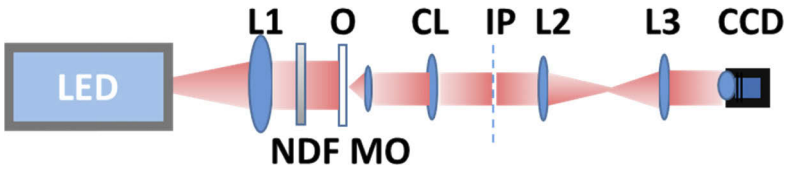

Fig. 3. (Color online) Schematic diagram of optical setup(L1, condenser lens; NDF, variable neutral density filter; O, phase object; MO, microscopic objective; CL, collimating lens; IP, image plane; L2-L3, 4f imaging relay system; CCD, camera).

shown below. First, a single micro-lens as shown in Figs. 4(a-c) has been taken to demonstrate the method. Figures 4(a), (b) and (c) show the focused intensity images at different levels of illumination conditions. In the reduced conditions, satisfactory phase images of the micro-lens have been retrieved. Similarly, the method has been tested for micro-lens array and onion's peel. As seen from Figs. 5 and 6, respectively, once again, acceptable phase results are obtained in low illumination conditions. The SNR has been determined on logarithmic manner using the following Eq. (14) where A_{ideal} is the original image and A_{noisy} is the noisy image.

$$SNR = 20\log\frac{||A_{ideal}||_F}{||A_{ideal} - A_{noisy}||_F} \tag{14}$$

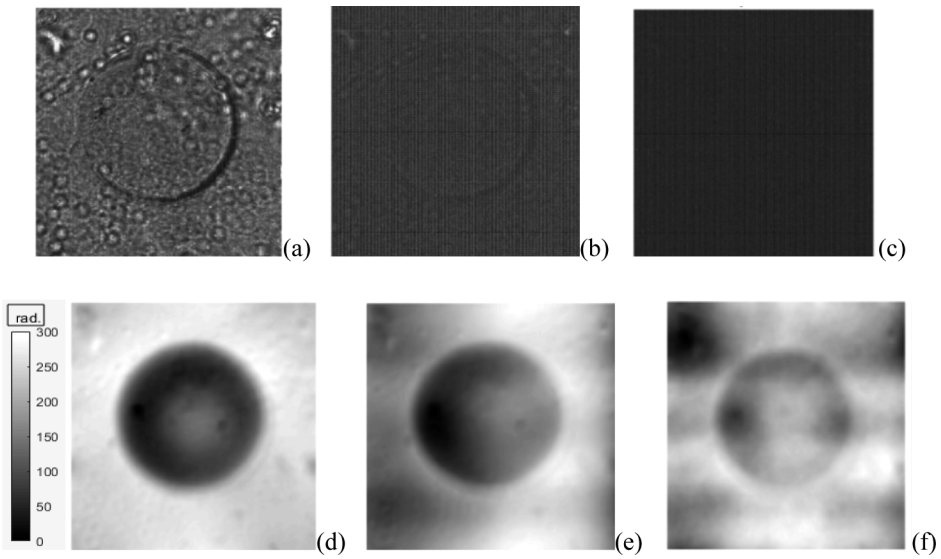

Fig. 4. Micro-lens: (a), (b), and (c) focussed images recorded on camera in varying photon-limiting conditions, viz., no photon limiting, SNR 7.2 and SNR 6.7, respectively; (d), (e), and (f) retrieved phase of (a), (b), and (c), respectively.

In simulation study, the number of photons has been taken as 10^5 and 10^4, which affected the visibility of the image drastically and therefore the SNRs were reduced to 1.0316 and 0.1032, respectively. Through the simulation results as shown in Figs. 1 and 2, it can be observed that phase images have been retrieved with relevant information even in such low SNR conditions. As we decrease the illumination intensity in our experiments by NDF, the SNRs of the resulted images also decreaseto7.26 and 6.74,respectively. The phase image retrieval with up to an SNR of 6 has previously been reported [19]. There is a good scope in the proposed TIE based

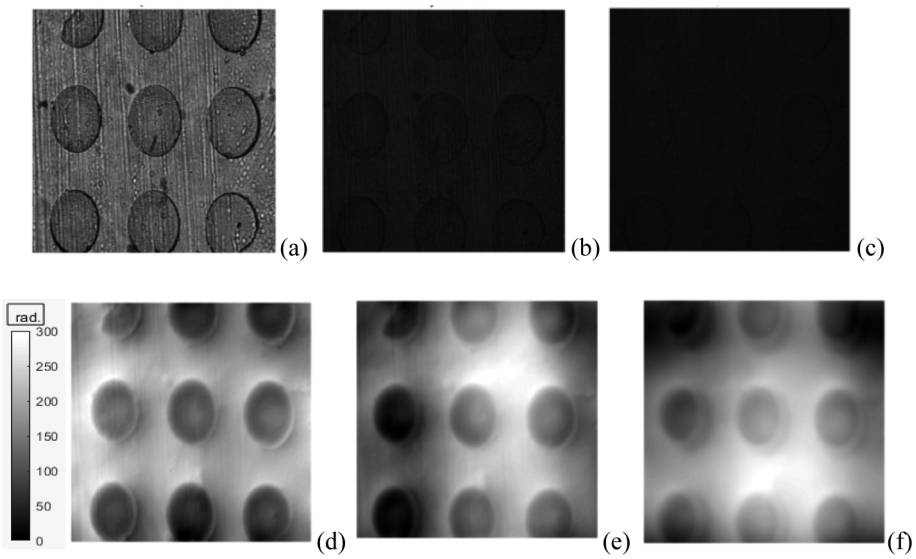

Fig. 5. Micro-lens array: (a), (b), and (c) focussed images recorded on camera in varying photon-limiting conditions, viz., no photon limiting, SNR 7.2 and SNR 6.7, respectively; (d), (e), and (f) retrieved phase of (a), (b), and (c), respectively.

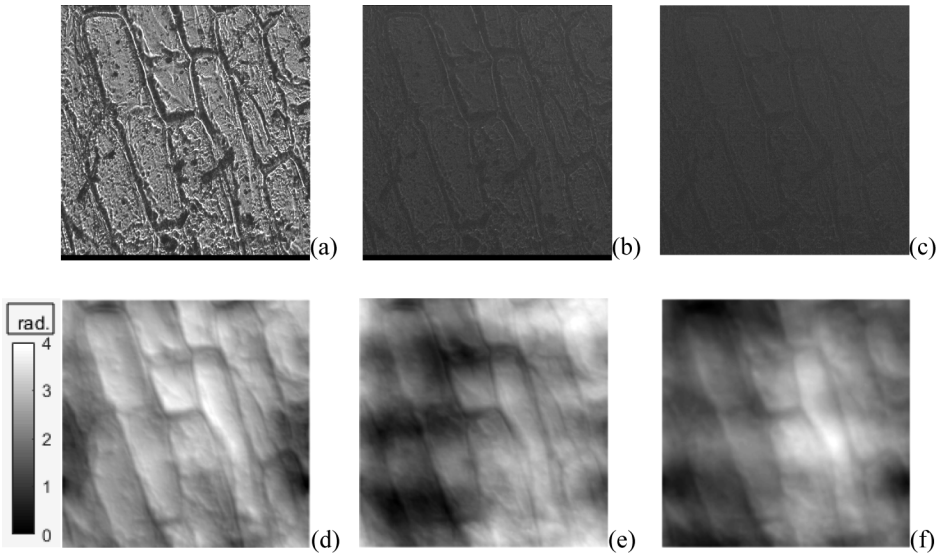

Fig. 6. Onion's peel: (a), (b), and (c) focussed images recorded on camera in varying photon-limiting conditions, viz., no photon limiting, SNR 7.2 and SNR 6.7, respectively; (d), (e), and (f) retrieved phase of (a), (b), and (c), respectively.

photon-counting phase imaging for enhancing the phase sensitivity and consequently phases retrieval for even lower SNR values in experiments; this will be pursued in the future.

OSA CONTINUUM

4. Conclusions

We have proposed and demonstrated photon-counting phase imaging based on TIE with large defocusing. It has been numerically shown that TIE can perform phase imaging using sufficiently large defocusing distances for photon-limited illumination. As a proof-of-concept, experimental results with three different phase objects using photon-limited partially coherent illumination have been presented, and experimental results are in agreement with our numerical simulations. Rigorous quantitative assessment of the quality of the phase retrieval based on properties of the partially coherent source [32] will be pursued in the future. For applications in astronomy and non-invasive imaging, different methods of TIE-based on this work can likely be used in the future for enhancing the capability of phase retrieval.

Acknowledgment

Mr. Rouchin Mahendra from IRDE Dehradun, India is acknowledged for providing micro-lens array.

Disclosures

The authors declare no conflicts of interest.

References

1. F. Zernike, "How I discovered phase contrast," Science **121**(3141), 345–349 (1955).
2. G. Popescu, L. P. Deflores, J. C. Vaughan, K. Badizadegan, H. Iwai, R. R. Dasari, and M. S. Feld, "Fourier phase microscopy for investigation of biological structures and dynamics," Opt. Lett. **29**(21), 2503–2505 (2004).
3. N. K. Nishchal, J. Joseph, and K. Singh, "Fully phase encryption using digital holography," Opt. Eng. **43**(12), 2959–2966 (2004).
4. D. P. Kelly, T. Meinecke, N. Sabitov, S. Sinzinger, and J. T. Sheridan, "Digital holography and phase retrieval: a theoretical investigation," Proc. SPIE **8074**, 807401 (2011).
5. D. Kumar and N. K. Nishchal, "Synthesis and reconstruction of multi-plane phase-only Fresnel holograms," Optik **127**(24), 12069–12077 (2016).
6. I. Muniraj, C. Guo, R. Malallah, J. P. Ryle, J. J. Healy, B.-G. Lee, and J. T. Sheridan, "Low photon count based digital holography for quadratic phase cryptography," Opt. Lett. **42**(14), 2774–2777 (2017).
7. R. A. Gonsalves, "Phase retrieval and diversity in adaptive optics," Opt. Eng. **21**(5), 829–832 (1982).
8. R. G. Paxman, T. J. Schulz, and J. R. Fienup, "Joint estimation of object and aberration by using phase diversity," J. Opt. Soc. Am. A **9**(7), 1072–1085 (1992).
9. J. Fienup, "Phase retrieval algorithms: a personal tour," Appl. Opt. **52**(1), 45–56 (2013).
10. Y. Shechtman, Y. C. Eldar, O. Cohen, H. N. Chapman, J. Miao, and M. Segev, "Phase retrieval with application to optical imaging: A contemporary overview," IEEE Signal Process. Mag. **32**(3), 87–109 (2015).
11. M. R. Teague, "Deterministic phase retrieval: a Green's function solution," J. Opt. Soc. Am. **73**(11), 1434–1441 (1983).
12. N. Streibl, "Phase imaging by the transport equation of intensity," Opt. Commun. **49**(1), 6–10 (1984).
13. T. E. Gureyevand K and A. Nugent, "Rapid quantitative phase imaging using the transport of intensity equation," Opt. Commun. **133**(1-6), 339–346 (1997).
14. L. Waller, L. Tian, and G. Barbastathis, "Transport of intensity phase amplitude imaging with higher order intensity derivatives," Opt. Express **18**(12), 12552–12561 (2010).
15. C. Zuo, Q. Chen, L. Tian, L. Waller, and A. Asundi, "Transport of intensity phase retrieval and computational imaging of partially coherent fields: The phase space perspective," Opt. Lasers Eng. **71**, 20–32 (2015).
16. M. Basunia, P. P. Banerjee, U. Abeywickrema, T.-C. Poon, and H. Zhang, "Recursive method for phase retrieval using transport of intensity and its applications," Appl. Opt. **55**(33), 9546–9554 (2016).
17. X. Meng, H. Huang, K. Yan, X. Tian, W. Yu, H. Cui, Y. Kong, L. Xue, C. Liu, and S. Wang, "Smartphone based hand-held quantitative phase microscope using the transport of intensity equation method," Lab Chip **17**(1), 104–109 (2017).
18. W.-J. Zhou, X. Guan, F. Liu, Y. Yu, H. Zhang, T.-C. Poon, and P. P. Banerjee, "Phase retrieval based on transport of intensity and digital holography," Appl. Opt. **57**(1), A229–A234 (2018).
19. K. Komuro, Y. Yamazaki, and T. Nomura, "Transport of intensity computational ghost imaging," Appl. Opt. **57**(16), 4451–4456 (2018).
20. R. L. Lucke and L. J. Rickard, "Photon-limited synthetic-aperture imaging for planet surface studies," Appl. Opt. **41**(24), 5084–5095 (2002).

OSA CONTINUUM

21. G. Pedrini, A. Faridian, A. K. Singh, and W. Osten, "Phase retrieval for optical metrology," Proc. SPIE **9276**, 927602 (2014).
22. J. Rosen and G. Brooker, "Digital spatially incoherent Fresnel holography," Opt. Lett. **32**(8), 912–914 (2007).
23. I. Rasnik, T. French, K. Jacobson, and K. Berland, "Electronic cameras for low, light microscopy," Methods Cell Biol. **114**, 211–241 (2013).
24. M. Yamamoto, H. Yamamoto, and Y. Hayasaki, "Photon-counting digital holography under ultraweak illumination," Opt. Lett. **34**(7), 1081–1083 (2009).
25. T. J. Gould and J. Bewersdorf, "Nanoscopy at low light intensities shows its potential," eLife **1**, e00475 (2012).
26. I. Testa, N. T. Urban, S. Jakobs, C. Eggling, K. L. Willig, and S. W. Hell, "Nanoscopy of living brain slices with low light levels," Neuron **75**(6), 992–1000 (2012).
27. Y. Chen, Y. Zou, P. Huang, J. Qi, W. He, and Q. Chen, "Reconstruction algorithm of low-light integral imaging by electron-multiplying charge-coupled device," Opt. Eng. **58**(5), 1 (2019).
28. K. Yan, L. Lifei, D. Xuejie, Z. Tongyi, L. Dongjian, and Z. Wei, "Photon-limited depth and reflectivity imaging with sparsity regularization," Opt. Commun. **392**, 25–30 (2017).
29. A. Goy, K. Arthur, S. Li, and G. Barbastathis, "Low photon count phase retrieval using deep learning," Phys. Rev. Lett. **121**(24), 243902 (2018).
30. D. Paganin and K. A. Nugent, "Noninterferometric phase imaging with partially coherent light," Phys. Rev. Lett. **80**(12), 2586–2589 (1998).
31. C. Zuo, Q. Chen, W. Qu, and A. Asundi, "Noninterferometric single-shot quantitative phase microscopy," J. Microsc. **38**(18), 3538–3541 (2013).
32. J. Petruccelli, L. Tien, and G. Barbastathis, "The transport of intensity equation for optical path length recovery using partially coherent illumination," Opt. Express **21**(12), 14430–14441 (2013).
33. D. Paganin, A. Barty, P. J. McMahon, and K. A. Nugent, "Quantitative phase amplitude microscopy III. The effect of noise," J. Micros. **214**(1), 51–61 (2004).
34. S. W. Hasinoff, F. Durand, and W. T. Freeman, "Noise optimal capture for dynamic range photography," *Proc. IEEE Computer Society Confer. on Computer Vision and Pattern Recognition*, San Francisco, USA, 553–560 (2010).
35. S. Yeom, B. Javidi, and E. Watson, "Photon counting passive 3D image sensing for automatic target recognition," Opt. Express **13**(23), 9310–9330 (2005).
36. P. Latorre-Carmona, B. Javidi, F. Pla, and E. Tajahuerce, "Photon counting 3-D object recognition using digital holography," IEEE Photonics J. **5**(6), 6900309 (2013).
37. S. K. Rajput, D. Kumar, and N. K. Nishchal, "Photon counting imaging and polarized light encoding for secure image verification and hologram watermarking," J. Opt. **16**(12), 125406 (2014).
38. S. K. Rajput and N. K. Nishchal, "Optical asymmetric cryptosystem based on photon counting and phase-truncated Fresnel transforms," J. Mod. Opt. **64**(8), 878–886 (2017).